MICHAEL E. THOMAS and RICHARD I. JOSEPH

THE INFRARED PROPERTIES OF POLAR CRYSTALS

Current applications of optical window materials require a comprehensive characterization of the index of refraction and the absorption coefficient as functions of frequency and temperature. General models of one- and multiphonon processes are used to describe the complex index of refraction of polar crystals in the infrared.

INTRODUCTION

Research and development concerning optical materials has greatly increased over the past five years, driven by the technological growth of highly sensitive detectors, optical communication systems, infrared imaging systems, and dual-mode infrared and microwave systems, in addition to technological requirements for improved fiber-optic materials, high-power laser windows, and windows for high-velocity vehicles. All this greater interest demands increased levels of material performance and characterization.

APL has been involved over the past few years in the effort to characterize optical materials more completely.[1-3] To illustrate the scope of the endeavor, Fig. 1 shows the index of refraction from 10^{-3} to 10^2 and the absorption coefficient from 10^{-5} to 10^7 over seven orders of magnitude in wave number (reciprocal wavelength) for a typical polar crystalline material at room temperature. The temperature dependence of the index of refraction and the absorption coefficient must be known from absolute zero to the material's melting temperature.

Such a comprehensive understanding of the optical properties of materials is simply not available today. But a considerable effort on selected pieces of the optical properties problem is represented in the literature.[4-15] Our goal is to put these pieces together and fill in the gaps to obtain a comprehensive picture.

Because most optical windows are on the order of 1 mm to 1 cm thick, the transparent region begins when the absorption coefficient is below 1 cm^{-1}. The material can be used as a window in the regions of transparency and as a narrow-band reflector in the opaque regions. Two window regions (far infrared and infrared/visible) typically exist within the optical spectrum of a polar crystal, as shown in Figs. 1a and 1b. The window regions, characterized by nearly constant refractive indexes, are determined by the strength and position of the lattice vibrations and electronic band transitions. The electronic band transitions influence ultraviolet and visible windows, and the lattice vibrations influence directly the far-infrared and infrared windows. APL's characterization effort has concentrated primarily on the lattice vibrations. In our investigation, a theoretically founded model containing experimentally determined optical
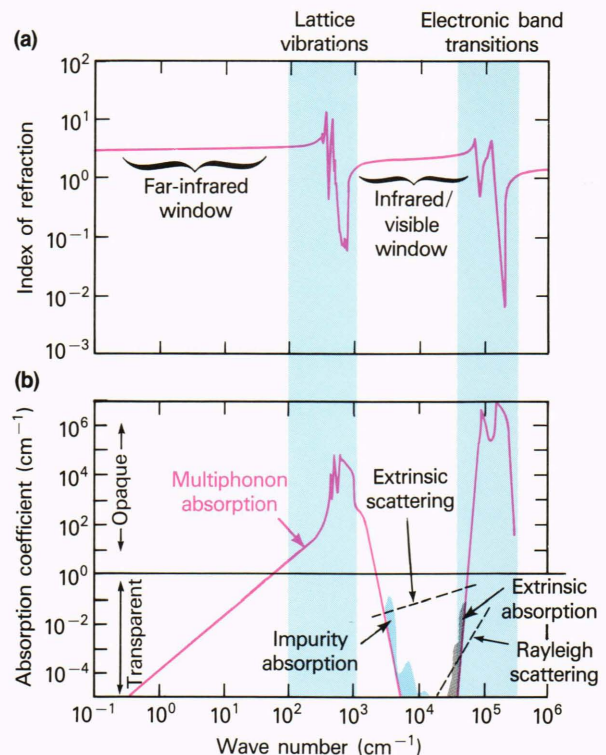

Figure 1—Optical properties of a typical polar crystalline material.

constants is used to characterize the index of refraction and absorption coefficient as functions of frequency and temperature.[2,3]

The usefulness of this new modeling is demonstrated in the following examples. High-power laser windows feature a phenomenon called thermal lensing (this will also be true for high-power microwave sources). Although the absorption coefficient may be very low, the laser power is sufficiently high to cause considerable window heating. The window temperature will not be uniform, because of the beam profile and thermal conduction. The temperature gradient causes an index gradient across the window and results in a lensing effect, which can degrade beam focus or collimation and therefore degrade the performance of a system. If the temperature-

328

dependent optical properties are understood, then compensation can be designed properly. Another example is fiber-optic materials for communication. To realize the lowest loss, extrinsic absorption and scatter must be minimized. When extrinsic effects are made sufficiently small, the optimum absorption coefficient will occur at the frequency where the multiphonon absorption edge and Rayleigh scattering intersect. In some materials (e.g., fluoride glasses), the intersection occurs at such low absorption levels that a repeaterless transatlantic fiber-optic communication link is possible if extrinsic losses are greatly reduced.

We present in this article an overview of theoretical models used to characterize the optical properties and a description of the experimental techniques and apparatus used to measure the optical constants of materials. Results of the characterization are applied to selected oxides, fluorides, sulfides, and alkali halides.

BACKGROUND

In an absorbing medium, the frequency-dependent complex dielectric constant ϵ can be represented by

$$\epsilon(\omega) = \epsilon_1 + i\epsilon_2 = (n^2 - \kappa^2) + i(2n\kappa), \quad (1)$$

where n is the index of refraction and κ is the index of extinction. The magnitude of the reflectance of a medium (at normal incidence) is then given by

$$|R| = \frac{(n-1)^2 + \kappa^2}{(n+1)^2 + \kappa^2}. \quad (2)$$

Generally, a measurement of $|R|$ is not sufficient to determine ϵ. Hence, it is necessary to describe the form of the complex dielectric constant. The "classical model" represents ϵ in the form

$$\epsilon(\omega) = \epsilon_\infty + \sum_j \frac{\Delta\epsilon_j \omega_j^2}{\omega_j^2 - \omega^2 + i\omega\gamma_j}. \quad (3)$$

The sum is over all long-wavelength infrared-active modes. Here, ω_j is the long-wavelength transverse-optic-mode frequency, $\Delta\epsilon_j$ is the mode strength, γ_j is the mode line width, and ϵ_∞ is ϵ (visible). The static dielectric constant $\epsilon_s = \epsilon(0)$ is given by

$$\epsilon_s = \epsilon_\infty + \sum_j \Delta\epsilon_j. \quad (4)$$

This model satisfies the Kramers–Kronig relation and therefore provides the corrected relationship between ϵ_1 and ϵ_2. It also allows for the construction of a physically meaningful representation of ϵ, using only the magnitude of R as input.

The origin of Eq. 3 can be seen by considering a one-dimensional lattice of oppositely charged ions, as shown in Fig. 2a. The total potential energy (U) of this lattice comprises two parts:
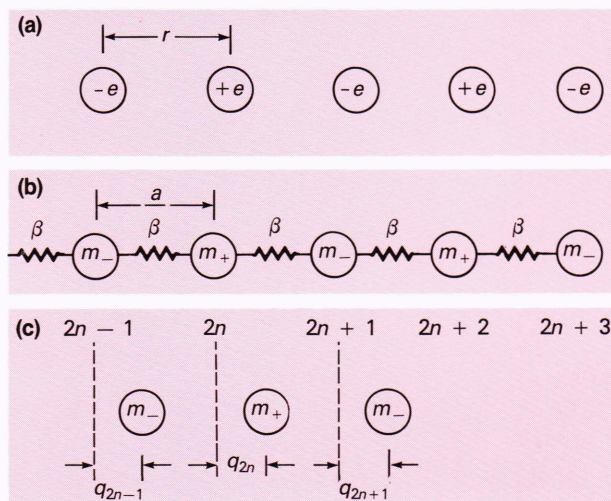

Figure 2—(a) A one-dimensional lattice of oppositely charged ions with spacing r; (b) charged ions of mass $m_\pm$ connected by springs with spring constant β; and (c) illustration of an equilibrium coordinate q.

$$U = -\frac{N\alpha e^2}{r} + \frac{NA}{r^m}, \quad (5)$$

where N is the number of ions per unit volume, A is a constant, α is the polarizability, and r is the spacing between ions. The first term in Eq. 5 represents the electrostatic attraction between the ions with charge e. Quantum-mechanical effects, which prevent the ions from overlapping, are represented by the second, very short-range ($m \approx 10$) repulsive term. Figure 3 shows this energy as a function of ion separation. Energy is at a minimum at a separation of $r = a$, the lattice constant. Near that minimum, $U \simeq (r - a)^2$, and the potential is harmonic (i.e., the force is proportional to $r - a$, giving Hooke's law). Ionic separations significantly far from $r = a$ create higher-order (anharmonic) force terms. We will discuss these effects in more detail later in this article.

Using a Hooke's law approximation, we can determine the normal vibrational modes of this lattice. Interionic forces are modeled as massless springs of spring constant β, as shown in Fig. 2b. Positive ions (mass m_+) are labeled by the indexes $2n$, negative ions (mass m_-) by $2n - 1$. The term q_j ($= r - a$) denotes the displacement of the jth ion from its equilibrium position, as shown in Fig. 2c. It follows directly from Newton's second law that the forces on the ions labeled $2n$ and $2n + 1$ are given by

$$F_{2n} = m_+ \frac{d^2 q_{2n}}{dt^2} = \beta(q_{2n+1} - 2q_{2n} + q_{2n-1})$$

and

$$F_{2n+1} = m_- \frac{d^2 q_{2n+1}}{dt^2} = \beta(q_{2n+2} - 2q_{2n+1} + q_{2n}). \quad (6)$$

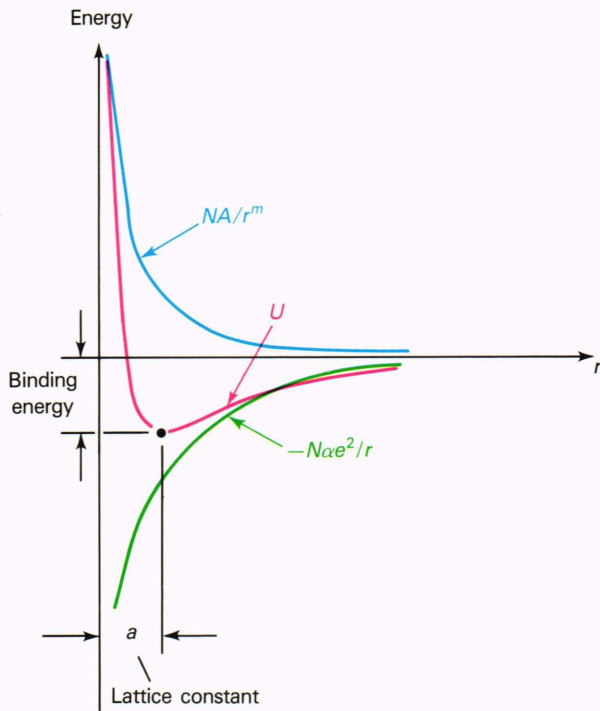These equations of motion can be solved by setting

Figure 3—The intramolecular potential between ions of opposite charge, showing both the attractive and repulsive potentials.

Figure 4—Dispersion curves for $m_+ > m_-$, showing both the optic and acoustic branches for a one-dimensional diatomic crystal lattice (see Eq. 8).

$$q_{2n} = \zeta \exp [i(\omega t - 2nka)]$$

and

$$q_{2n+1} = \eta \exp\{i[\omega t - (2n + 1)ka]\} , \quad (7)$$

where ζ and η are amplitude factors and $k = 2\pi/\lambda$, with λ being a wavelength. Substitution of Eq. 7 into Eq. 6 then gives the dispersion relation

$$\omega^2 = \beta\left(\frac{1}{m_+} + \frac{1}{m_-}\right) \pm \beta\left[\left(\frac{1}{m_+} + \frac{1}{m_-}\right)^2 - \frac{4}{m_+ m_-} \sin^2 ka\right]^{1/2} . \quad (8)$$

Equation 8 has two types of solutions (branches). Figure 4 shows a plot of ω versus k for $m_+ \geq m_-$. The lower branch is known as the acoustic branch, the upper one as the optic branch. The names of the branches come from examining the ratio ζ/η as $k \to 0$ ($\lambda \to \infty$). For the acoustic branch, $\zeta/\eta \to 1$, so that all ions move in the same direction. This motion can be stimulated by external forces such as sound waves. For small values of k, ω/k is the velocity of sound (V_s) in the material. For the optic branch, when $k \to 0$, $\zeta/\eta \to -(m_-/m_+)$, and the oppositely charged ions move in opposition to each other. This kind of motion can be excited by an electric field (i.e., electromagnetic [optical] radiation). For the lattice to respond to an electromagnetic wave, the wave and the lattice vibration must have the same
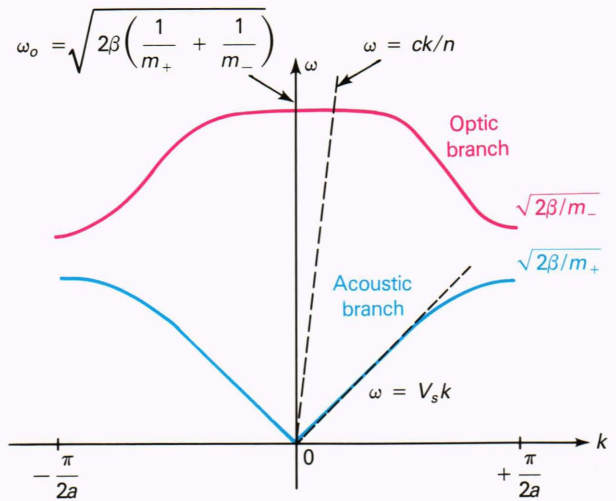
frequency and wavelength. The dispersion relation for electromagnetic radiation is $\omega = ck/n$, where c is the velocity of light in the medium. This dispersion relation is also shown in Fig. 4. Because of the large value of the speed of light compared with the speed of sound ($c/V_s \approx 10^5$), the optic branch and lattice dispersions intersect very near $k = 0$ on the scale of $\pi/2a$.

When an electric field $E = E_0 e^{i\omega t}$ is applied, the equations of motion, Eq. 6, become

$$m_+ \frac{d^2 q_{2n}}{dt^2} = \beta(q_{2n+1} - 2q_{2n} + q_{2n-1}) + eE_0 e^{i\omega t} \quad (9a)$$

and

$$m_- \frac{d^2 q_{2n+1}}{dt^2} = \beta(q_{2n+2} - 2q_{2n+1} + q_{2n}) + eE_0 e^{i\omega t}. \quad (9b)$$

Assuming solutions for q_{2n} and q_{2n+1} of the same form as given in Eq. 7, we find that for $k \approx 0$,

$$\eta = \frac{-(e/m_-)E_0}{\omega_0^2 - \omega^2}$$

and

$$\zeta = \frac{(e/m_+)E_0}{\omega_0^2 - \omega^2} , \quad (10)$$

both representing the motion of an oscillator to a driving frequency, ω.

In a real lattice, the vibrations are not independent but are coupled to one another because of anharmonicities

330

in the potential energy and other effects thus far ignored. These effects lead to energy dissipation through lattice waves (called phonons) of finite lifetimes, and may be represented phenomenologically by introducing a damping term that represents a force, opposed to the ionic motion and proportional to the velocity. Consequently, adding the terms $-m_+\gamma(dq_{2n}/dt)$ and $-m_-\gamma(dq_{2n+1}/dt)$ to the right side of Eqs. 9a and 9b, respectively, where γ is the damping factor, changes the solution of Eq. 10 to

$$\eta = \frac{-(e/m_-)E_0}{\omega_0^2 - \omega^2 + i\gamma\omega}$$

and

$$\zeta = \frac{(e/m_+)E_0}{\omega_0^2 - \omega^2 + i\gamma\omega} \ . \tag{11}$$

Electric dipoles can be constructed for each ion pair. Without an electric field, the ionic dipole moment per cell is zero. When a field is turned on, however, each cell acquires a dipole moment

$$p = e(\zeta - \eta) \ , \tag{12}$$

so that the lattice now has a net polarization

$$P = Np \ . \tag{13}$$

This result neglects the contribution of atomic polarizability, which, if added, gives

$$P = \epsilon_0 Ne(\zeta - \eta) + \epsilon_0 \chi_e E_0 \ . \tag{14}$$

Finally, writing for the electric displacement D,

$$D = \epsilon_0 \epsilon E_0 = \epsilon_0 E_0 + P \ , \tag{15}$$

we have

$$\epsilon = (1 + \chi_e) + \frac{4\pi Ne^2 \left(\dfrac{1}{m_+} + \dfrac{1}{m_-} \right)}{\omega_0^2 - \omega^2 + i\gamma\omega}$$

$$\equiv \epsilon_\infty + \frac{\omega_0^2 (\epsilon_s - \epsilon_\infty)}{\omega_0^2 - \omega^2 + i\gamma\omega} \ , \tag{16}$$

which is precisely of the form shown in Eq. 3 for one mode. We can represent χ_e in more detail by electronic transitions with the same classical model as that used to describe the lattice vibrations.

In a d-dimensional lattice with R atoms per unit cell, there generally will be d acoustic branches and $d(R-1)$ optic branches. The example just considered had $d = 1$

and $R = 2$, giving one optic branch and one acoustic branch. In a three-dimensional lattice, there generally are $3(R-1)$ optic branches. For example, in sapphire, where $R = 30$, there can be 87 optic branches, but not all of those branches are infrared-active. The number of infrared-active optic branches (in a material with no defects or impurities) can be determined using group theoretic methods. For example, in the ordinary ray of sapphire, there are four infrared-active modes.[16] Figure 5 shows a comparison between the measured room-temperature reflectivity of sapphire and that computed using Eqs. 2 and 3. Table 1 gives the values of the one-phonon parameters used in this fit[3] (e.g., ϵ_∞, $\Delta\epsilon_j$, ω_j [$= 2\pi c\nu_{TOj}$], γ_j, and ω_{LO} [$= 2\pi c\nu_{LO}$]). The term ω_{LO} is the longitudinal optical-mode frequency. (We will discuss the multiphonon parameters later in this article.)

HIGHER-ORDER THEORY

The heuristic derivation of the dielectric constant presented above is theoretically sound.[5,9,10] The detailed theory offers further significant insights that aid in describing the optical properties of polar crystals. Although we will not present the involved details of that theory here, it is important to note its starting point. Let Q denote a normal coordinate of the lattice. Q is proportional to the q discussed in the one-dimensional example previously described. Then the potential energy U caused by lattice displacements can generally be written in the form

$$U = U_h + U' \ ,$$

$$U_h = \frac{1}{2} \sum_i \omega_i^2 Q_i^2 \ ,$$

$$U' = \sum_{i,j,k} b_{ijk} Q_i Q_j Q_k$$

$$+ \sum_{i,j,k,l} c_{ijkl} Q_i Q_j Q_k Q_l + \dots \tag{17}$$

Here, U_h represents the harmonic and U' the anharmonic contribution; ω_i is the frequency of the ith mode, and the tensors b_{ijk} and c_{ijkl} are constants. Let M denote a component of the dipole moment vector caused by lattice displacements and Q_0 the normal coordinate of that optical mode with zero wave number whose polarization is in the same direction. If the ions were rigid, then

$$M = eQ_0 \left(N\left[\frac{1}{m_+} + \frac{1}{m_-} \right] \right)^{1/2} , \tag{18}$$

where e is the charge on an ion, N is the number of ion pairs, and $m_\pm$ denotes the masses of the positive and negative ions. The electron shells can be deformed during lattice vibration (by the dipolar field and short-range forces). The deformation follows the lattice displacements adiabatically and since it is a unique function of
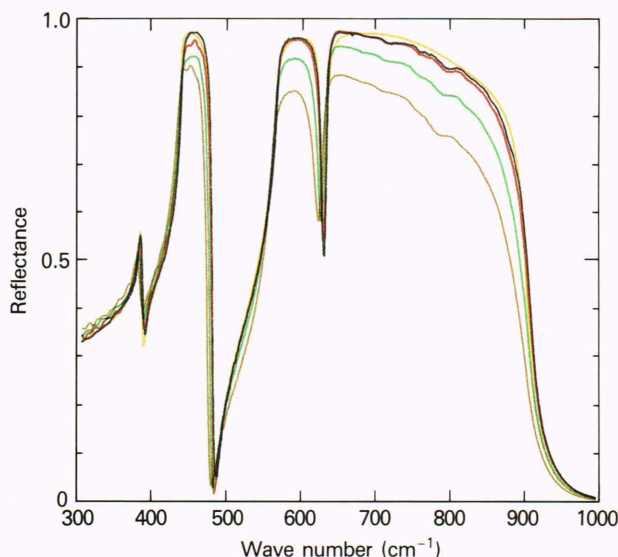
Figure 5—The reflectance of the ordinary rays of sapphire: black, measured (T = 295 K); yellow, modeled (T = 295 K); red, measured (T = 373 K); green, measured (T = 573 K); brown, measured (T = 773 K).

$$M = \alpha_0 Q_0 + \sum_{i,j} \beta_{ij} Q_i Q_j + \sum_{i,j,k} \gamma_{ijk} Q_i Q_j Q_k + \cdots ,$$
$$(19)$$

where α_0, β_{ij}, and γ_{ijk} are constants. The term α_0 contains both the effects of the displacement of the ions as a whole, as given by Eq. 18, and the first-order effect of the electronic distortions. The terms β_{ij} and γ_{ijk} are caused entirely by electronic deformation. Since the first-order moment of any lattice wave with finite wavelength must vanish when summed over a whole wave, only α_0 contributes to the first-order term. Finally, the total potential energy of a lattice is equal to $U - E_{ext} M$, where E_{ext} is the applied electric field.

The calculations of ϵ noted above[5,9,10] use only terms explicitly shown in Eqs. 17 and 19. Generally, when we include terms additional to the U_h and $\alpha_0 Q_0$ in $U - E_{ext} M$, the quantities $\Delta\epsilon_j$ and ω_j become linear functions of temperature in the classical limit. When we include terms proportional to the three Q's in U and the two Q's in M, the γ_j also have a linear temperature dependence. These results are in good accord with experimental observation and our own results. There is one further consequence: the γ_j's, in addition to being temperature-dependent, now become explicit functions of frequency, for example, $\gamma_j(\omega, T)$. The importance of this feature is discussed below.

MULTIPHONON PROCESSES

The two main mechanisms for intrinsic phonon absorption in pure solids are lattice vibrations at the fundamental frequency ω_0 and electronic transitions that occur above the material's band gap energy. The latter is in the ultraviolet, the former in the far infrared. Hence, the character of intrinsic infrared absorption is determined by the lattice vibrations. At frequencies above ω_0, the absorption process is dominated by the funda-

the lattice configuration, the dipole moment connected with it can also be expanded in a power series in the lattice displacements. The higher-order terms (in the Q's) contain cross terms between various lattice modes; therefore, a combination of two or more lattice waves can absorb in the infrared, even if the individual waves separately cannot. Consequently, in addition to the anharmonic terms in the potential, the higher-order terms in the dipole moment also provide a mechanism for absorption of a wide range of frequencies. Hence, when the dipole moment caused by electronic deformation is considered, M is no longer linear in the displacements, and takes the form

Table 1—Optical constants of sapphire (Al_2O_3).*

Material	One-Phonon Parameters (T = 295 K)						Multiphonon Parameters		
	ν_{TO} (cm^{-1})	$\Delta\epsilon$	γ/ν_{TO}	ν_{LO} (cm^{-1})	ϵ_o	ϵ_∞	ν_m (cm^{-1})	D/hc (cm^{-1})	K (cm^{-2})
Al_2O_3 (ordinary ray)[2,16,17]	385.0	0.30	0.015	388	9.39	1	914	14,000	1.436×10^7
	442.0	2.70	0.010	480					
	569.0	3.00	0.020	625					
	635.0	0.30	0.020	788					
	806.0	0.004	0.035	914					
	90,334.0†	1.058							
	162,738.0†	1.024							
Al_2O_3 (extraordinary ray)[16,18]	400.0	6.80	0.020	512	11.55	1	871	9800	8.164×10^6
	583.0	1.70	0.035	871					
	82,201.1†	0.551							
	135,082.6†	1.504							

*From Ref. 3. Reproduced by permission, Soc. Photo-Opt. Instrum. Eng.
†Electronic transitions.

mental lattice vibration (one phonon) and its higher harmonics, which are called multiphonon processes. At frequencies above $3\omega_0$, extrinsic material defects, impurities, and scattering usually become important.

The multiphonon absorption edge shifts to higher frequencies as the temperature is increased. The experimental characterization of both the temperature and frequency dependence of absorption usually requires a large number of measurements. Fortunately, there are theoretical models that accurately characterize the absorption, and those models require that only a few material-dependent parameters be determined.

The main criteria in choosing which of many multiphonon absorption models to use are simplicity, minimum number of adjustable parameters, and general applicability. Below, we describe results[2,11-15] based on the so-called Morse interatomic potential,

$$U(r) = D \{1 - \exp[-a(r - r_0)]\}^2 , \quad (20)$$

where D is the dissociation energy, r_0 is the location of the equilibrium position, $a = \omega_0(\mu/2D)^{1/2}$, ω_0 is the fundamental lattice vibrational frequency, and μ is the reduced mass. The Morse potential is used because it leads to an exact solution of the quantum-mechanical Schrödinger equation and includes anharmonic effects to all orders (although it assumes special relations regarding the size and type of the various anharmonic contributions). In addition to the form of U given above, the model calculations make other simplifying assumptions: that a single generalized dissociation energy is sufficient, and that no impurities or defects are present. In our approach, we will assume that, in the multiphonon region, the one-phonon density of states $\rho_1(\nu)$ vanishes above ν_m, the maximum longitudinal optical-mode frequency, and the n-phonon density of states $\rho_n(\nu)$ is of a Gaussian form involving certain statistical parameters.

The calculation of the resulting multiphonon absorption coefficient of $k(\omega, T)$ is complex. (The interested reader is referred to Ref. 2 for details.) The theoretical results depend on only three parameters: the dissociation energy D, the maximum single-phonon frequency ν_m (the maximum ν_{LO} in the material), and a scaling factor K. Figure 6 (Ref. 2) illustrates the structure of the total absorption coefficient k ($= 4\pi\nu\kappa$) in terms of $k_n(\nu, T)$, the absorption coefficient of a single n-phonon process. The individual k_n values are nearly Gaussian in shape, yet the sum $k = \Sigma k_n$ produces a nearly exponential curve of k, as observed experimentally.

Figure 7 (Ref. 3) is a plot of the absorption coefficient as a function of frequency in pure yttria at 295 K. Shown explicitly are theoretical results for the one-phonon contribution (red) and the multiphonon contribution (black). Unfortunately, the one-phonon contribution appears to dominate, and would destroy the fit of the experimental data to the multiphonon theory. The cause of this dilemma is that the form of the damping term in Eq. 3 (the one-phonon contribution to the α is proportional to the γ_j) cannot be strictly correct, since
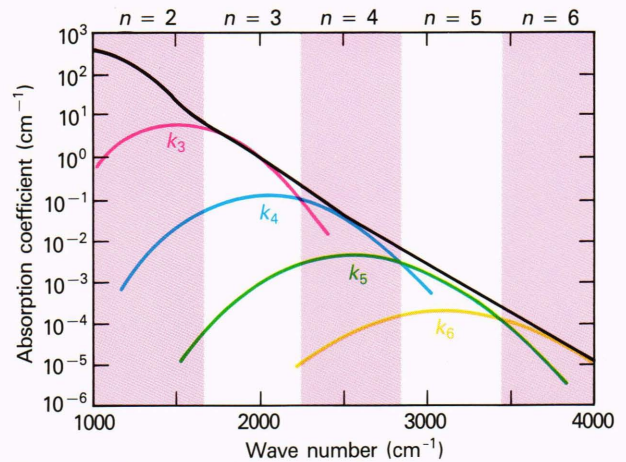

Figure 6—The n-phonon absorption regions for room-temperature sapphire. (From Ref. 2. Reproduced by permission, Opt. Soc. Am.)
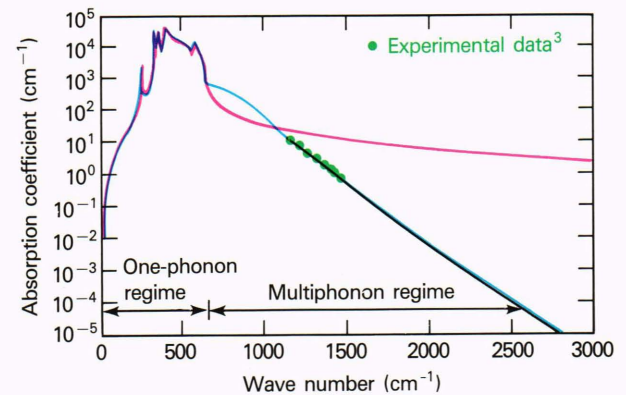

Figure 7—Absorption coefficient as a function of frequency for pure yttria at 295 K: red, one-phonon model (no cutoff); black, multiphonon model; and blue, all-phonon model. (From Ref. 3. Reproduced by permission, Soc. Photo-Opt. Instrum. Eng.)

it would grow larger as ω increases, a result contrary to both the experimental evidence and intuition. We have already alluded to the resolution of this difficulty in our previous discussion. When higher-order terms in U and M are included, γ itself becomes a function of ω. For cubic anharmonicities, $\gamma(\omega, T)$ is of the form $T\phi(\omega)$. A calculation of $\phi(\omega)$ requires detailed knowledge of the phonon density of states.[3] But $\phi(\omega)$ remains relatively constant at "low" frequencies and then decays rapidly to zero above the maximum longitudinal mode frequency. Without the detailed information necessary to compute $\gamma(\omega, T)$, the best one can do is to take a phenomenological approach. Hence, we replace Eq. 3 with

$$\epsilon(\omega) = \epsilon_\infty + \sum_j \frac{\Delta\epsilon_j \, \omega_j^2}{\omega_j^2 - \omega^2 + i\omega\gamma_j f(\omega)} , \quad (21)$$

where $f(\omega)$ is taken to be unity for frequencies where Eq. 3 gave a good fit to the data, and $f(\omega)$ is to decay rapidly to zero in the multiphonon region, effectively

removing the one-phonon contribution to the absorption coefficient. In particular, we have taken[3]

$$f(\omega) = \begin{cases} 1 & \omega \leq \bar{\omega} \\ \exp\{-\mu[(\omega/\bar{\omega})^2 - 1]\} & \omega \geq \bar{\omega} \end{cases}, \quad (22)$$

where μ and $\bar{\omega}$ are adjustable parameters. The blue curve in Fig. 7 corresponds to the values $\mu = 4$, $\bar{\omega} = 1.1$ times the highest-infrared-allowed transverse-optic-mode frequency. Thus, a continuous representation of the phonon absorption can be achieved.

EXPERIMENTAL DATA

We conducted both transmission and reflection measurements to characterize comprehensively the studied optical materials over a broad spectral region (100 to 5000 cm^{-1}). The transmission experiments are used to measure the multiphonon absorption characteristics, and the reflection measurements are used to measure the one-phonon (lattice vibration) characteristics.

A Fourier transform spectrometer (FTS) Bomem model DA3.02 was used for the transmission measurements. A ratio of the transmission results of two different thicknesses was used to reduce surface effects. Measurements were made between 2 and 20 μm (5000 and 500 wave numbers) using a liquid-nitrogen-cooled mercury–cadmium telluride detector. The entire optical train of the spectrometer was under vacuum during the experiment to eliminate unwanted atmospheric water vapor and carbon dioxide contamination, giving a clean spectrum. A Specac high-temperature absorption cell was adapted to the sample compartment of the FTS. The accuracy of the measured bulk extinction coefficient de-

pends on the baseline stability of the system. The time between the measurements of the two different sample thicknesses determines the stability. For room-temperature data, the time could be very short, and absorption coefficients accurate to within 0.002 cm^{-1} were obtained. But the heated samples required time for cooling and heating, since only one cell was available. That limitation reduced the accuracy of the high-temperature measurements by roughly an order of magnitude.

A Barnes model 500 specular reflectance device, adaptable to the Bomem spectrometer, was used for room-temperature reflectance measurements. Angles of incidence from 5° to 85° could be obtained. An aluminum mirror was used as a reference, but it did not have 100% reflectivity over the range of interest. Therefore, the baseline of reflectance usually required a mirror correction. Measurements were conducted with a germanium-on-potassium bromide beam splitter and a mercury–cadmium telluride detector, as well as with a Mylar beam splitter and a deuterated triglycerin sulfide detector. The low wave number limit was 100 cm^{-1}. These components allowed complete coverage of the *Reststrahlen* bands.

Temperature-dependent reflectance measurements also were conducted using the FTS. The sample compartment of the FTS was modified to contain the Specac heatable cell and the appropriate transfer optics (see Fig. 8), which are symmetrically designed with two spherical mirrors (focal length = 10.9 cm). The same sets of beam splitters and detectors were used as in the room-temperature measurements. The experiment began with a background measurement at room temperature (295 K) with an NRC ER.2 mirror. Then a sample was inserted into the cell and a reflection measurement was made. The cell was heated to 373 K and another reflection measurement was made. This process was repeated at 573 and 773 K. The cell was then allowed to cool, the mirror was reinserted,
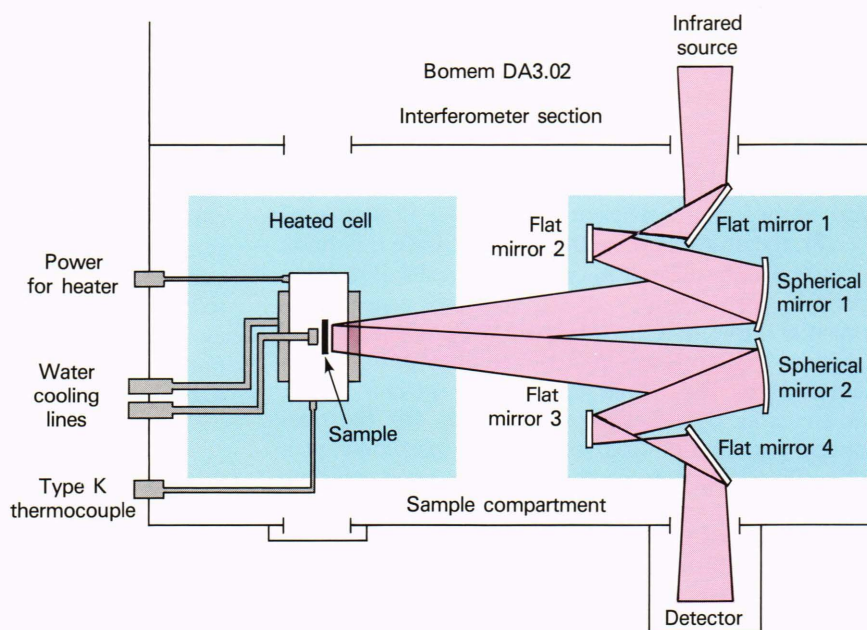

Figure 8—Optical design of transfer optics (focal length of spherical mirrors = 10.9 cm).

and a final background was obtained. The entire process took about two hours. The error in the experiment was ±3%.

An adjustable parallel-plate capacitor was designed and constructed to accept 2.54-cm-diameter disks of variable thicknesses. A Hewlett–Packard model 4275A LCR meter was used for impedance measurements. The meter accounted for background impedance; thus, a purely capacitive load was observed. The measurements were made at 100 kHz. In this way, the static relative permittivity was measured for each material ($C = \epsilon_s A/d$, where C is the capacitance, A is the area of the sample, and d is the thickness of the sample). Although the accuracy was only ±10%, it was sufficient for the initial parameters.

RESULTS

We applied the models discussed above with reasonable success to oxides, fluorides, and alkali halides.[3] Materials were characterized by several parameters from both the one-phonon and multiphonon models. We did not attempt to obtain optimum fits to the experimental data, but the limits of the models and the errors in the experimental data were reasonably matched. An exception was the index of refraction, n, in the transparent regime of a few materials. When extremely accurate experimental data existed for the index, we did not optimize the parameters to represent the data. Accurate models representing the data already existed in limited spectral regions, and our emphasis was on broad spectral coverage.

The parameters that characterize sapphire (Al_2O_3) are listed in Table 1 for both the ordinary and extraordinary rays. The experimental data used to determine the parameters were obtained from measurements at APL and from the literature. We give a few representative figures to demonstrate the quality of the fit of the model and its comprehensive nature. Figures 9 and 10 (Ref. 2) as well as Fig. 11 present the absorption coefficient as a function of frequency and temperature for selected oxides. Comparing the model and experimental data, one sees excellent agreement. Figure 11 illustrates a limitation of the model: in some materials, such as fused silica, pronounced two-phonon structures are observed, and the assumption of a Gaussian phonon distribution is violated. To some degree, this model inaccuracy occurs in all materials, and a more detailed representation is needed to describe this region accurately. Also, impurity absorption (OH^-) occurs, and scattering is evident. These are extrinsic features that vary from sample to sample, and are therefore hard to model reliably.

The phonon distribution function $\rho_n(\nu)$ contains statistical parameters representing the mean α_1, standard deviation α_2, and skewness α_3. Surprisingly, these parameters change very little from one class of materials to the next, but some variation was necessary, and the parameters are listed in Table 2.

The index of refraction is dominated by a one-phonon process, so only the one-phonon model is used for index computations. The model is consistent with the Sellmeier model for $\gamma = 0$. The Sellmeier model is commonly used in the literature; the electronic transitions, when available, can be obtained from those references. But the representation of the phonon (vibrational) modes is frequently incomplete, and the joining of the electronic parameters with the complete phonon parameters from a different source degrades the quality of the fit, as illustrated in Table 3 (Ref. 3). The index accuracy obtained from the APL model ranges about ±0.003, whereas the limited Sellmeier model used by Malitson[23] achieves an accuracy in the range of ±0.00002. This limitation is caused not by the model but by the accuracy and consistency of the data used to derive model parameters.

The model can be used to compute the index of refraction as a function of frequency, and the multiphonon absorption coefficient as a function of frequency and temperature; those quantities can then be used to compute total emissivity, dispersion ($dn/d\lambda$), and thermal effects. This aspect of the model's utility has been very advantageous in our design efforts using oxides.

As previously discussed, a theoretical basis exists for the temperature dependence of one-phonon processes. But parameters in the models must be determined experimentally by reflection spectra as functions of temperature. Current efforts at APL seek to do precisely those experimental measurements.

Figure 5 shows typical reflectance spectra for sapphire at four temperatures (295, 373, 573, and 773 K). The structures in the spectra shift to lower frequencies and broaden as the temperature increases. On the basis of

Table 2—Statistical parameters for the phonon distribution function.

Material	α_1	α_2	α_3
Quartz	0.510	0.140	0.052
Alkali halides	0.530	0.145	0.052
All others	0.537	0.153	0.052

Table 3—Index of refraction of barium fluoride.*

ν (cm^{-1})	$n_{observed}$[23]	$n_{calculated}$ (APL model)	$\Delta n = n_{observed} - n_{calculated}$
3881.1	1.46262	1.4598	0.0028
3740.0	1.46234	1.4595	0.0028
2922.2	1.45940	1.4569	0.0025
1946.3	1.45012	1.4486	0.0015
1802.1	1.44732	1.4462	0.0011
1603.1	1.44216	1.4417	0.0005
1419.6	1.43529	1.4356	− 0.0031
1028.4	1.40514	1.4093	− 0.0042
966.6	1.39636	1.4017	− 0.0053

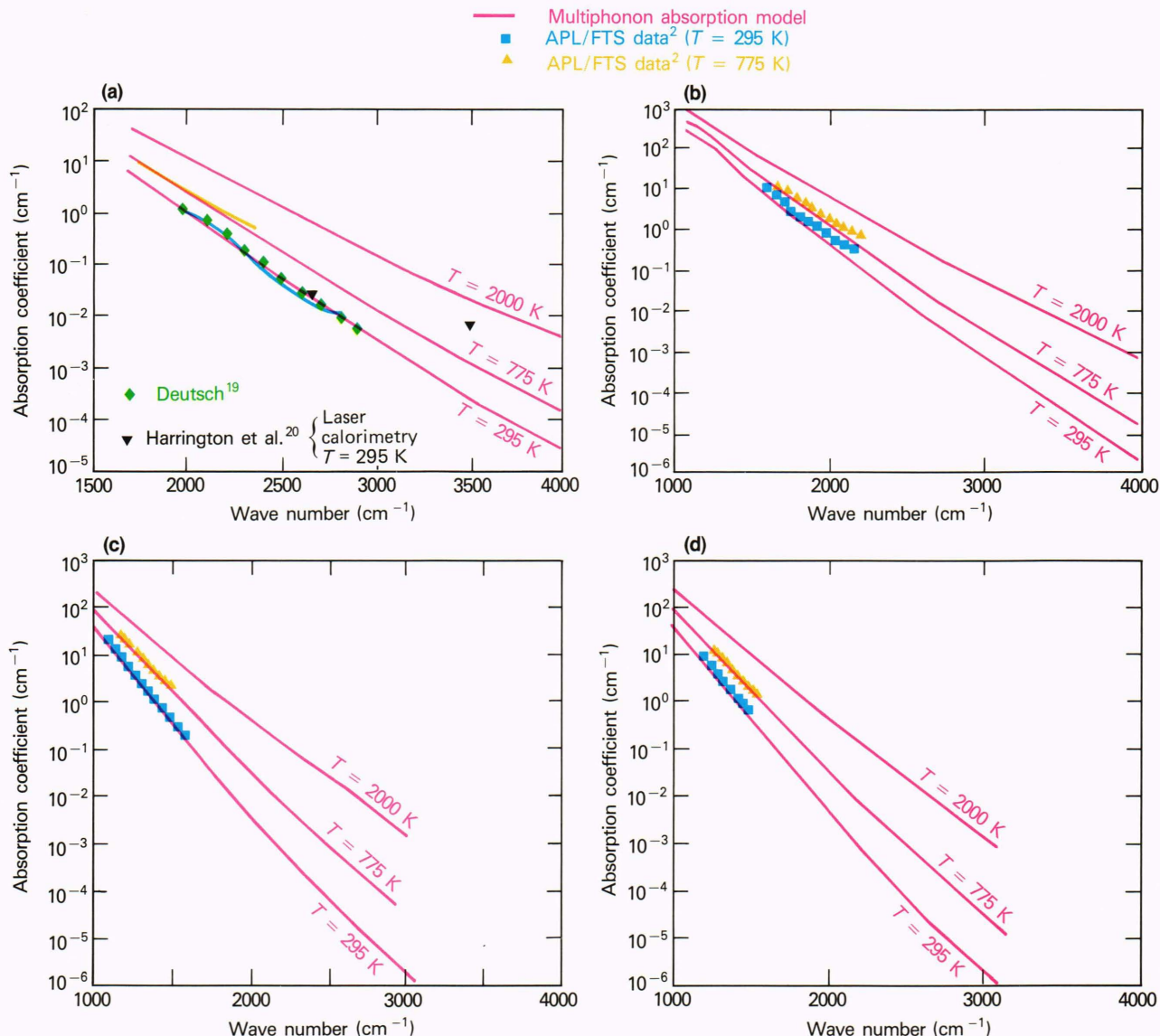*From Ref. 3. Reproduced by permission, Soc. Photo-Opt. Instrum. Eng.

Figure 9—The absorption coefficient versus wave number. A comparison between experimental data and the multiphonon model at various temperatures for (a) sapphire, (b) spinel, (c) lanthina-doped yttria, and (d) pure yttria. (From Ref. 2. Reproduced by permission, Opt. Soc. Am.)

the theories previously reviewed, the temperature dependence is linear in a high-temperature approximation ($hc\nu_j/kT \leq 1$, where h is Planck's constant and ν_j is the optical-mode wave number). The transverse optical-mode shifts can be modeled by the simple formula

$$\nu_{TOj}(T) = \nu_{TOj}(T_0) - a_j(T - T_0) , \qquad (23)$$

where T is the temperature and a_j is a coefficient. The results of applying this formula to sapphire are shown in Fig. 12. A linear trend is clear over the entire temperature range measured, and should continue to higher temperatures according to theory, but not necessarily to lower temperatures.

The damping factor γ_j (see Eq. 3) increases with increasing temperature as given by

$$\gamma_j(T) = \gamma_j(T_0) + b_j(T - T_0) , \qquad (24)$$

where b_j is a coefficient. Again, this trend is observed in the data and should continue to higher temperatures according to theoretical prediction.

The strength of the modes is represented by $\Delta\epsilon_j$. The true temperature dependence of $\Delta\epsilon_j$ can be masked by the choice of temperature dependence of γ_j. Thus, a measurement of ϵ independent of γ must be made. This can be done by examining the static dielectric constant ϵ_s (see Eq. 4). Figure 13 shows the temperature dependence of ϵ_s for sapphire. Note that at high temperatures the dependence is linear. Again, this trend should continue, on the basis of theory.[9] Thus, the complex dielectric constant (and complex index of refraction $n = \sqrt{\epsilon}$) can be meaningfully extrapolated as a function of temperature.
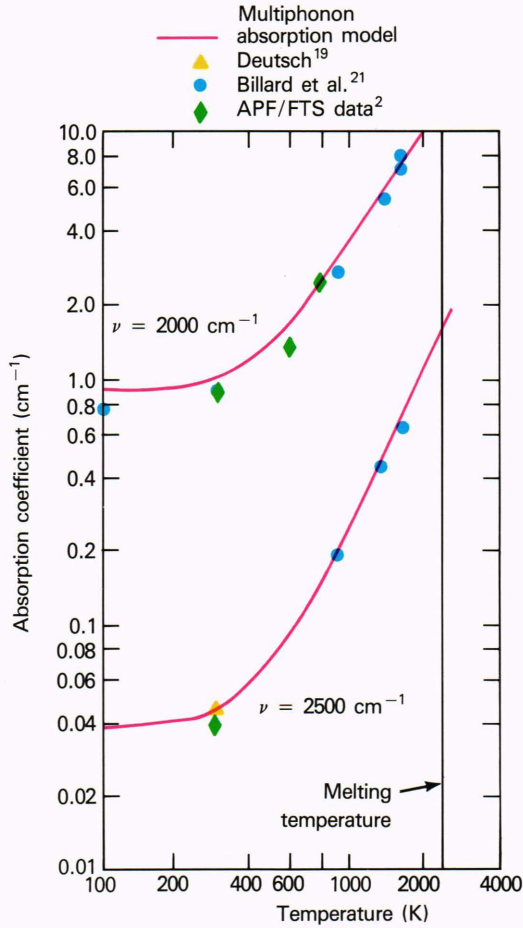
Figure 10—Absorption coefficient versus temperature for sapphire. (From Ref. 2. Reproduced by permission, Opt. Soc. Am.)
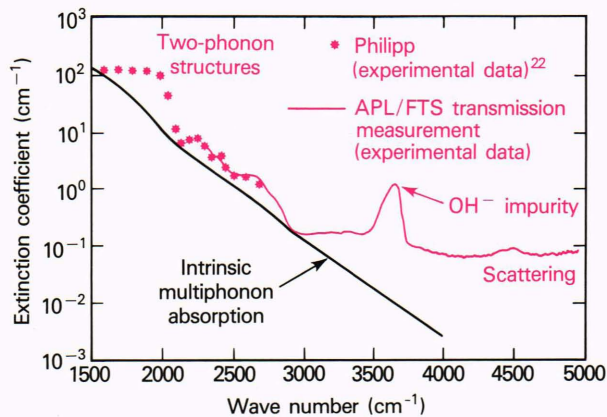

Figure 11—Fused silica extinction coefficient at $T = 295$ K for experimental data and the multiphonon absorption model.

Figure 12—The temperature dependence of the transverse optical modes of sapphire (ν_{TO} versus temperature).

$$\nu_{TO4} = 639.2 - 1.46 \times 10^{-2} T$$
$$\nu_{TO3} = 570.5 - 1.35 \times 10^{-2} T$$
$$\nu_{TO2} = 440.6 - 1.06 \times 10^{-2} T$$
$$\nu_{TO1} = 384.1 - 1.26 \times 10^{-2} T$$
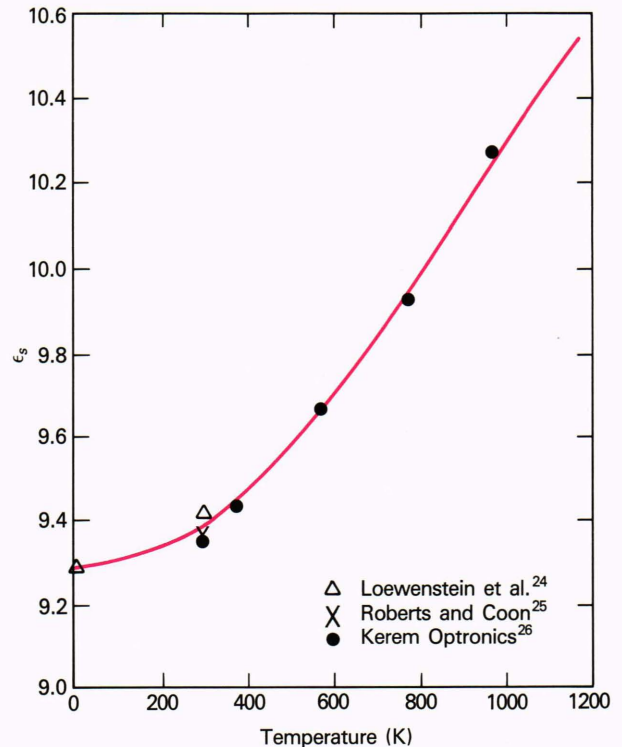
Figure 13—The temperature dependence of the static dielectric constant (ϵ_s) of sapphire.

CONCLUSIONS

We have presented a simple, comprehensive model that allows the optical characterization of oxides, fluorides, sulfides and selenides, and alkali halides over a wide range of frequencies and temperatures. In the one-phonon region, the model is limited to room temperature, but the multiphonon model is valid up to the melting temperature of the material. We are now working
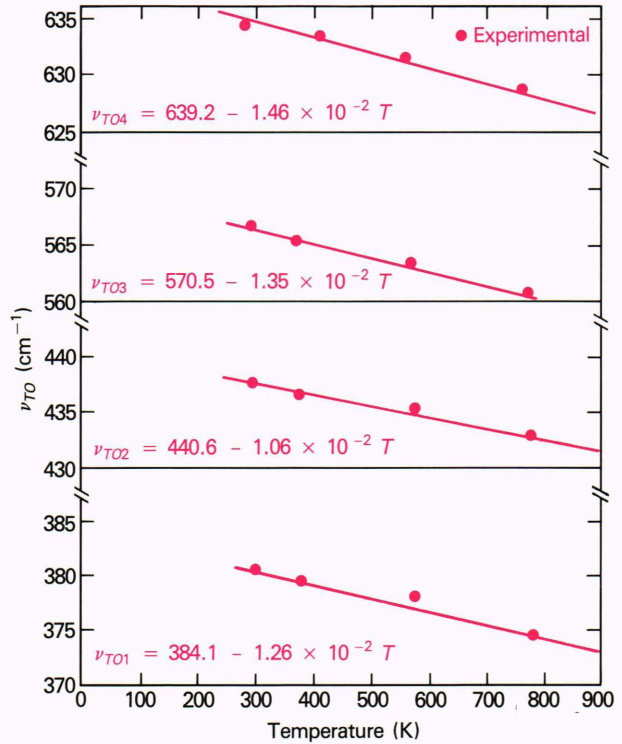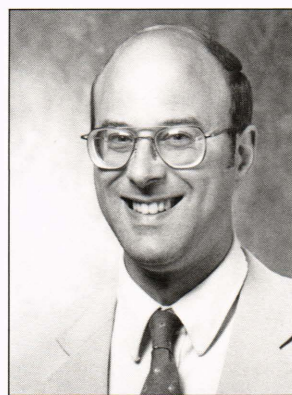
to characterize the temperature dependence of the one-phonon region. The major limitation of the model is its inability to characterize accurately the optical constants in the two-phonon region when the assumed statistical description of the phonon distribution function cannot adequately model the observed structure. The importance of this limitation depends on the material. In particular, quartz and ALON have pronounced features that are not well modeled.

We expect that the efforts reported here will be useful to many engineers and scientists who want to use transparent infrared materials to their maximum potential.

REFERENCES

[1] R. I. Joseph and M. E. Thomas, "Differential Reflection Spectroscopy: A Direct Determination of Long Wavelength Optical Mode Frequencies in Polar Crystals," *Phys. Status Solidi B* **141**, K163–K166 (1987).
[2] M. E. Thomas, R. I. Joseph, and W. J. Tropf, "Infrared Transmission Properties of Sapphire, Spinel, Yttria and ALON as a Function of Temperature and Frequency," *Appl. Opt.* **27**, 239–245 (1988).
[3] M. E. Thomas and R. I. Joseph, "A Comprehensive Model for the Intrinsic Transmission Properties of Optical Windows," *Proc. Soc. Photo-Opt. Instrum. Eng.* **929**, 87–93, *Infrared Optical Materials* (1988).
[4] A. A. Maradudin and R. F. Wallis, "Lattice Anharmonicity and Optical Absorption in Polar Crystals: II. Classical Treatment in the Linear Approximation," *Phys. Rev.* **123**, 777–789 (1961).
[5] R. F. Wallis and A. A. Maradudin, "Lattice Anharmonicity and Optical Absorption in Polar Crystals: III. Quantum Mechanical Treatment in the Linear Approximation," *Phys. Rev.* **125** 1277–1282 (1962).
[6] M. Born and K. Huang, *Dynamic Theory of Crystal Lattices*, Oxford University Press, New York (1956).
[7] R. W. H. Stevenson, ed., *Phonons in Perfect Lattices and in Lattices with Point Imperfections*, Oliver & Boyd, Edinburgh, Scotland (1966).
[8] S. S. Mitra and B. Bendow, eds., *Optical Properties of Highly Transparent Solids*, Plenum Press, New York (1975).
[9] B. Szigetti, "Higher-Order Terms in the Dielectric Constant of Ionic Crystals," *Proc. Roy. Soc.* **252**, 217–235 (1959).
[10] V. V. Mitskevich, "Infrared Absorption and Dispersion in LiF and MgO," *Fiz. Tverd. Tela.* **4**, 3035 (1962) [English translation: *Sov. Phys.—Solid State* **4**, 2224 (1963)].
[11] D. L. Mills and A. A. Maradudin, "Theory of Infrared Absorption by Crystals in the High Frequency Wing of Their Fundamental Lattice Absorption," *Phys. Rev. B* **8**, 1617–1630 (1973).
[12] A. A. Maradudin and D. L. Mills, "Temperature Dependence of the Absorption Coefficient of Alkali Halides in the Multiphonon Regime," *Phys. Rev. Lett.* **31**, 718–721 (1973).
[13] L. L. Boyer, J. A. Harrington, M. Hass, and H. B. Rosenstock, "Multiphonon Absorption in Ionic Crystals," *Phys. Rev. B* **11**, 1665–1679 (1975).
[14] H. B. Rosenstock, "Multiphonon Absorption in Alkali Halides: Quantum Treatment of Morse Potential," *Phys. Rev. B* **9**, 1963–1970 (1974).
[15] M. Sparks and L. J. Sham, "Theory of Multiphonon Absorption in Insulating Crystals," *Phys. Rev. B* **8**, 3037–3047 (1973).
[16] A. S. Barker, Jr., "Infrared Lattice Vibrations and Dielectric Dispersion in Corundum," *Phys. Rev.* **132**, 1474–1484 (1963).
[17] I. H. Malitson, "Refraction and Dispersion of Synthetic Sapphire," *J. Opt. Soc. Am.* **52**, 1377–1379 (1962).
[18] I. H. Malitson and M. J. Dodge, "Refractive Index and Birefringence of Synthetic Sapphire," *J. Opt. Soc. Am.* **62**, 1405A (1972).
[19] T. F. Deutsch, "Absorption Coefficient of Infrared Laser Window Materials," *J. Phys. Chem. Solids* **14**, 2091–2104 (1973).
[20] J. A. Harrington, D. A. Gregory, and W. F. Otto, Jr., "Infrared Absorption in Chemical Laser Window Materials," *Appl. Opt.* **15**, 1953–1959 (1976).
[21] D. Billard, F. Gervais, and B. Piriou, "Analysis of Multiphonon Absorption in Corundum," *Phys. Status Solidi B* **75**, 117–126 (1976).
[22] H. R. Philipp, "Silicon Dioxide (SiO_2) (Glass)," in *Handbook of Optical Constants*, E. D. Palik, ed., Academic Press Handbook Series, New York (1985).
[23] I. H. Malitson, "Refractive Properties of Barium Fluoride," *J. Opt. Soc. Am.* **54**, 628–632 (1964).
[24] E. V. Loewenstein, D. R. Smith, and R. L. Morgan, "Optical Constants of Far Infrared Materials. 2: Crystalline Solids," *Appl. Opt.* **12**, 398–406 (1973).
[25] S. Roberts and D. D. Coon, "Far Infrared Properties of Quartz and Sapphire," *J. Opt. Soc. Am.* **52**, 1023–1029 (1962).
[26] Kerem Optronics, Manufacturers Data Sheet, Industrial Area, P.O. Box 32, Dimona 86100, Israel.
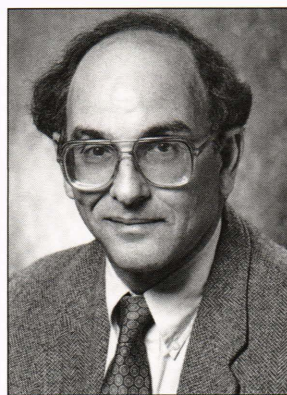
THE AUTHORS

MICHAEL E. THOMAS was born in Dayton, Ohio, in 1951. He received a B.S.E.E. degree from the University of Dayton in 1973 and M.S.E.E. (1976) and Ph.D. (1979) degrees from Ohio State University. He joined APL in 1979 and is with the Electro-Optical Systems Group of APL's Fleet Systems Department. In 1982, Dr. Thomas was a postdoctoral fellow in the Department of Physics, Naval Postgraduate School. He is a member of the Society of Photo-Optical Instrumentation Engineers, the Optical Society of America, and a senior member of IEEE. Since joining APL, he has been working his way up the electromagnetic spectrum, beginning with extremely low frequencies, then microwaves, and now visible and infrared frequencies. His current work includes characterization and modeling of atmospheric propagation, infrared window materials, and high-pressure gases.

RICHARD I. JOSEPH was born in Brooklyn in 1936. He received a B.S. from the City College of the City University of New York in 1957 and a Ph.D. from Harvard University in 1962, both in physics. From 1961 to 1966, he was a senior scientist with the Research Division of the Raytheon Co. Since 1966, Dr. Joseph has been with the Department of Electrical and Computer Engineering of The Johns Hopkins University, where he is currently the Jacob Suter Jammer Professor of Electrical and Computer Engineering. During 1972, Dr. Joseph was a Visiting Professor of Physics at the Kings College, University of London, on a Guggenheim Fellowship. A member of APL's Principal Professional Staff, his research interests include electromagnetic theory, solid-state theory, statistical mechanics, the theory of nonlinear evolution equations, and oceanography. Dr. Joseph is a Fellow of the American Physical Society.